NUMERICAL SIMULATION OF THE FLOW ABOUT AN F-18 AIRCRAFT IN THE HIGH-ALPHA REGIME

Scott M. Murman
MCAT Institute, Moffett Field, CA

Yehia M. Rizk
NASA Ames Research Center, Moffett Field, CA

Presented at
NASA 4th High Alpha Conference
July 12-14, 1994
Dryden Flight Research Facility

The current research is aimed at developing and extending numerical methods to accurately predict the high Reynolds number flow about the NASA F-18 HARV at large angles of attack. The resulting codes are validated by comparison of the numerical results with in-flight aerodynamic measurements and flow visualization obtained on the HARV. Further, computations have been used to provide an analysis and numerical optimization of a pneumatic slot blowing concept, and a mechanical strake concept, for use as potential forebody flow control devices in improving high-alpha maneuverability (cf. Gee, et al. These proceedings).

MOTIVATION

* PROVIDE FLIGHT-VALIDATED NUMERICAL METHODS FOR COMPUTING THE FLOW ABOUT AIRCRAFT OPERATING IN THE HIGH-APLHA REGIME

* USE THESE METHODS TO PROVIDE AN ANALYSIS AND OPTIMIZATION OF NEW CONTROL CONCEPTS FOR HIGH-ALPHA MANEUVERABILITY

Computation of the flow about the F–18 HARV at high alpha provides a challenge for numerical methods because of the complex physics involved and the complex geometry of a full-aircraft configuration. Since the computations are carried out to match actual flight operating conditions, the Navier-Stokes equations must be solved. Further, the flow about the majority of the aircraft is turbulent, and the computations must include suitable turbulence models. These models must be applied in a rational manner to account for the massive 3–D separation that occurs at large incidence. The complex aircraft geometry is modeled using structured, overlapped grids in what is termed a Chimera approach. This method allows grids to be generated about the separate components of the aircraft and then combined, greatly simplifying the grid generation procedure. This approach also allows the use of different numerical schemes in different regions of the aircraft, depending upon the physics encountered.

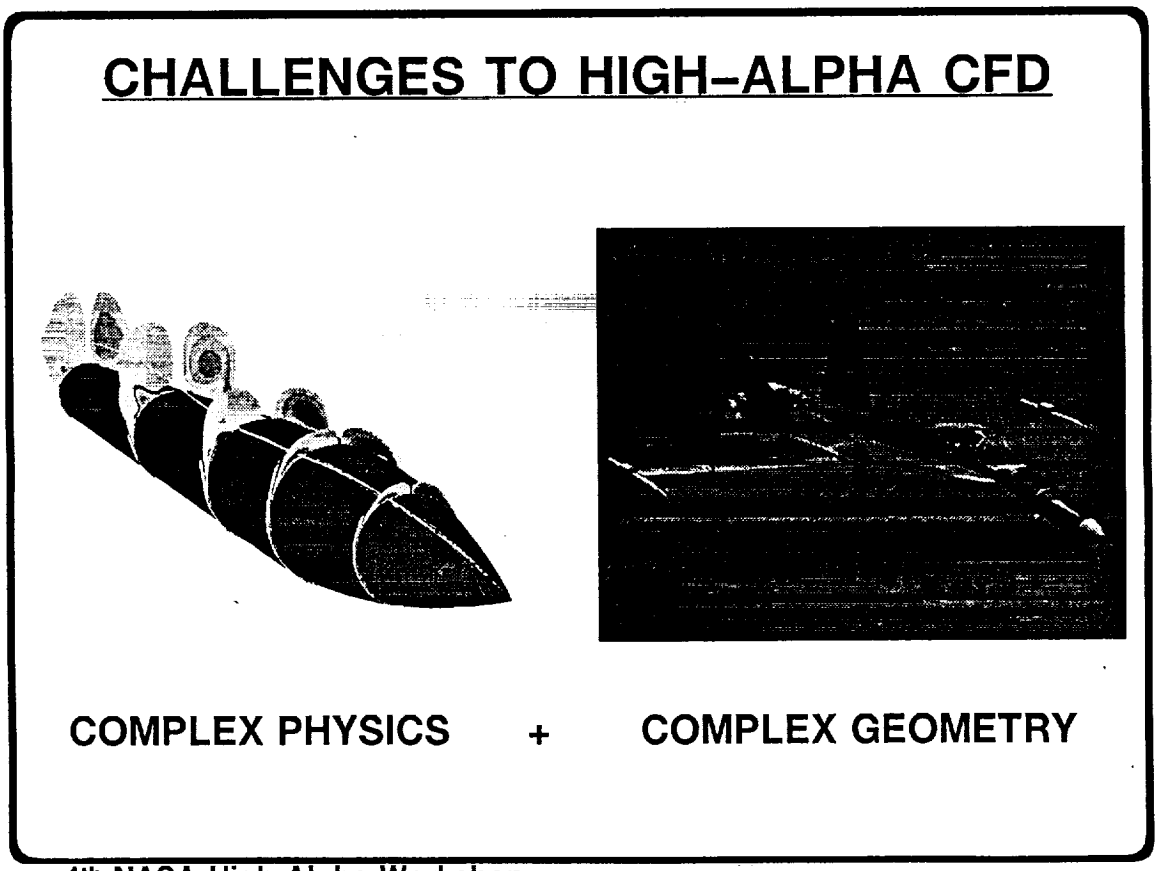

The computational model of the F–18 HARV is a continuing evolution of previous models. The current model has a finer grid spacing in the fuselage and LEX regions, and resolves the engine inlet region is greater detail. The figure shows the separate grids about the major components of the aircraft and how they overlap in the Chimera approach. The model contains 1.7 million grid points in 14 separate zones (15 zones for the $\alpha = 45°$ computations). It models all of the major components of the HARV, including the LEX, wing and leading-edge flap, and the horizontal and vertical tails. The wing-leading-edge flap and horizontal stabilizer are both scheduled with angle of attack in the computations.

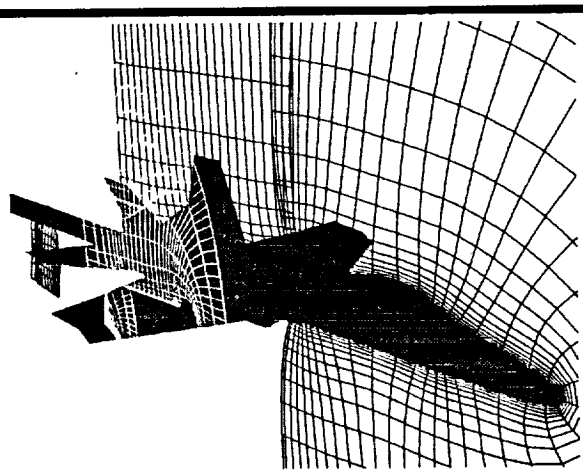

CURRENT F–18 COMPUTATIONAL MODEL

* 1.7 MILLION GRID POINTS FOR A SYMMETRIC COMPUTATION
* 14 STRUCTURED ZONES (13 NAVIER–STOKES)
* MODELS LEX, EMPENNAGE, DEFLECTED FLAP, AND INLET REGION
* MATCHES IN–FLIGHT ENGINE MASS FLOW RATES

This figure shows a close-up view of the engine inlet region of the HARV computational geometry. The major details of the region are modeled, including the boundary layer diverter and vent, and the engine cowling and diffuser. At the engine compressor face, a nozzle is added which forces the flow to choke at the throat of the nozzle. In this manner, different engine inlet mass flow rates can be simulated by opening or constricting the throat of this nozzle. The current computations are carried out at the maximum engine power setting in all cases ($\approx$ 60 lbm/sec per engine).

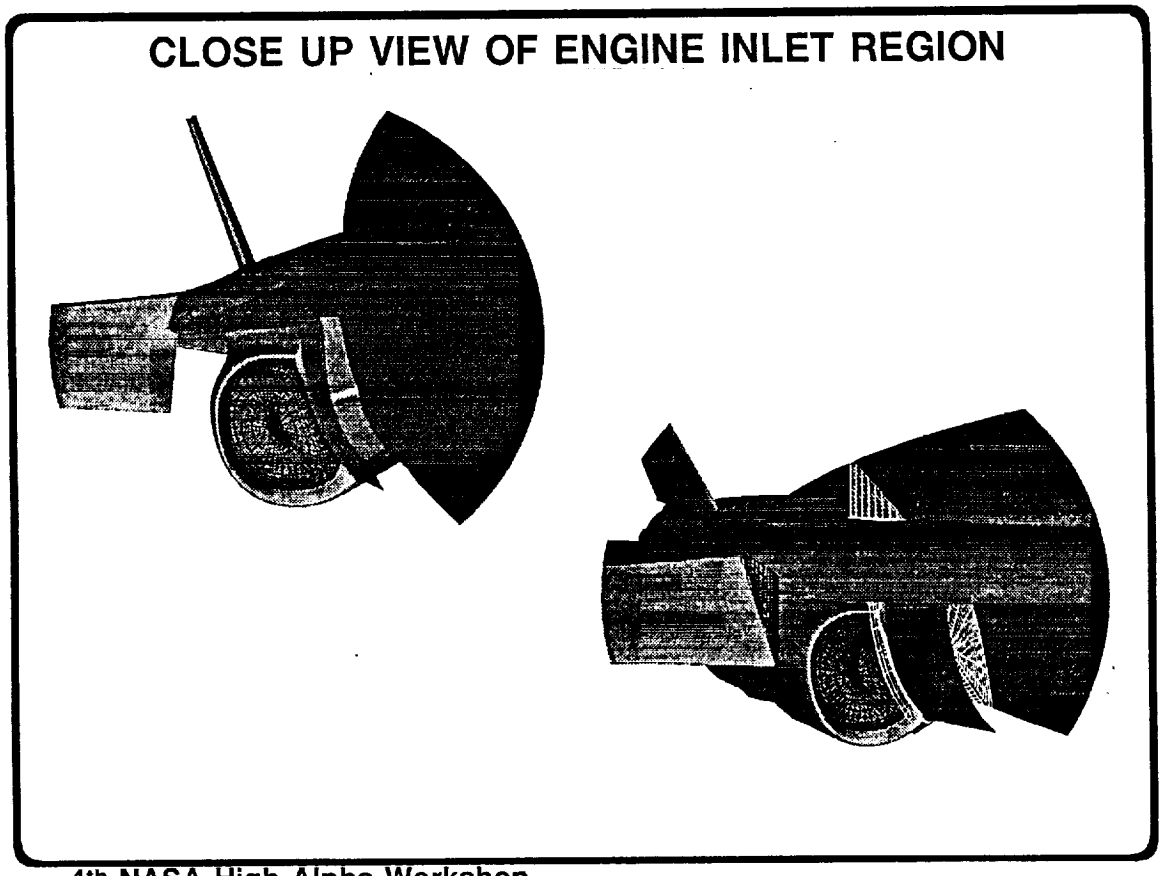

This view graph compares the computed and flight-test oil-flow patterns on the F–18 forebody and LEX at $\alpha = 30°$. The computations were carried out using the full-aircraft configuration. The HARV oil-flow pattern shows the lines of primary and secondary crossflow separation on the fuselage forebody. A primary crossflow separation occurs at the leading edge of the LEX, and the oil flow photo shows lines of secondary and tertiary separation on the upper surface of the LEX. The current computation shows an improvement in the resolution of the forebody secondary separation in comparison to that of a previous solution. The current computation also resolves the details of the secondary and tertiary separation patterns on the leeward side of the LEX. In addition, details of an additional primary and secondary crossflow separation pattern located on the side of the fuselage under the LEX can be seen in the present solution.

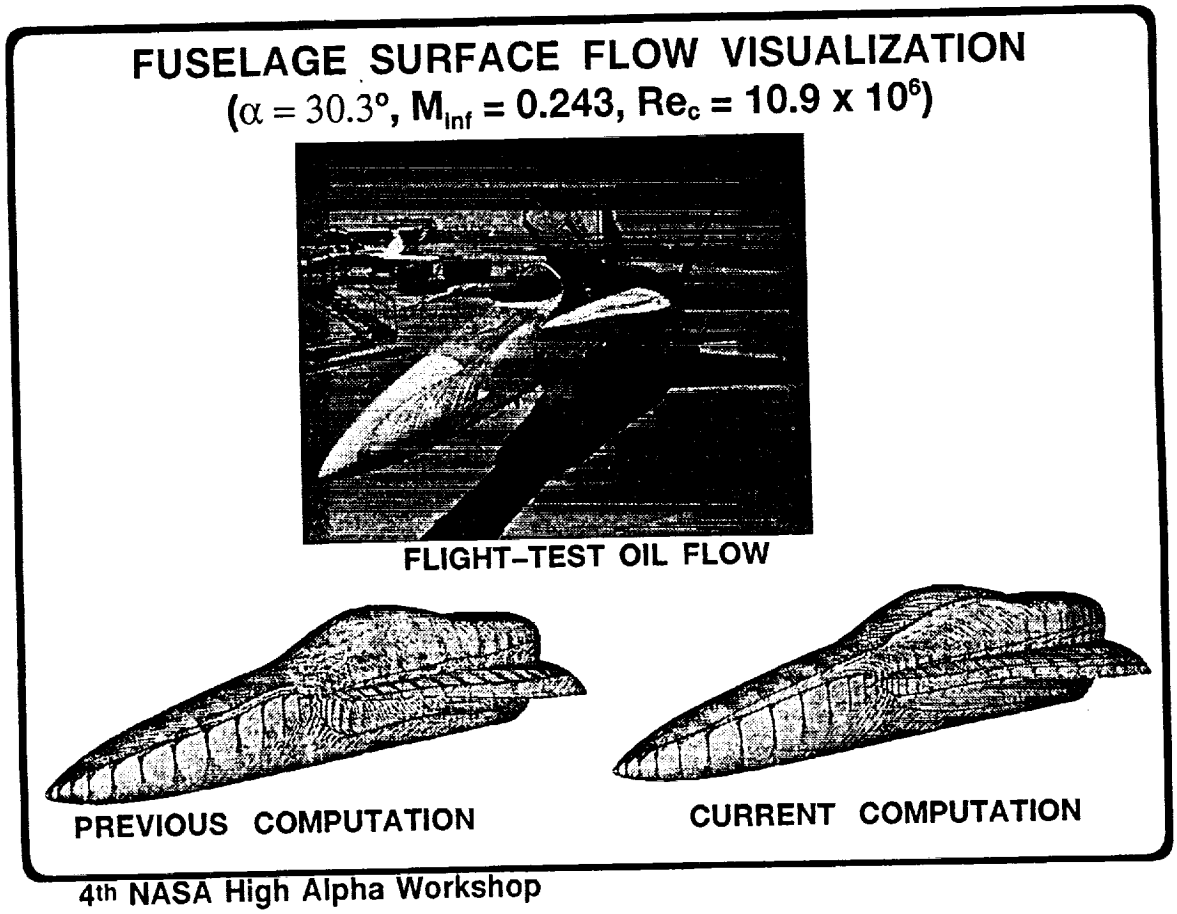

Particle trajectories (instantaneous streaklines) released from the tip of the forebody and the apex of the LEX in the present $\alpha = 30°$ computation show the path of the forebody and LEX vortices. The flight-test smoke flow visualization is shown for comparison. The slow expansion of the vortex core upstream of breakdown, and the loss of core structure starting in the vicinity of the LEX-wing junction can be seen. The computed vortex breakdown occurs slightly further downstream than is observed in flight.

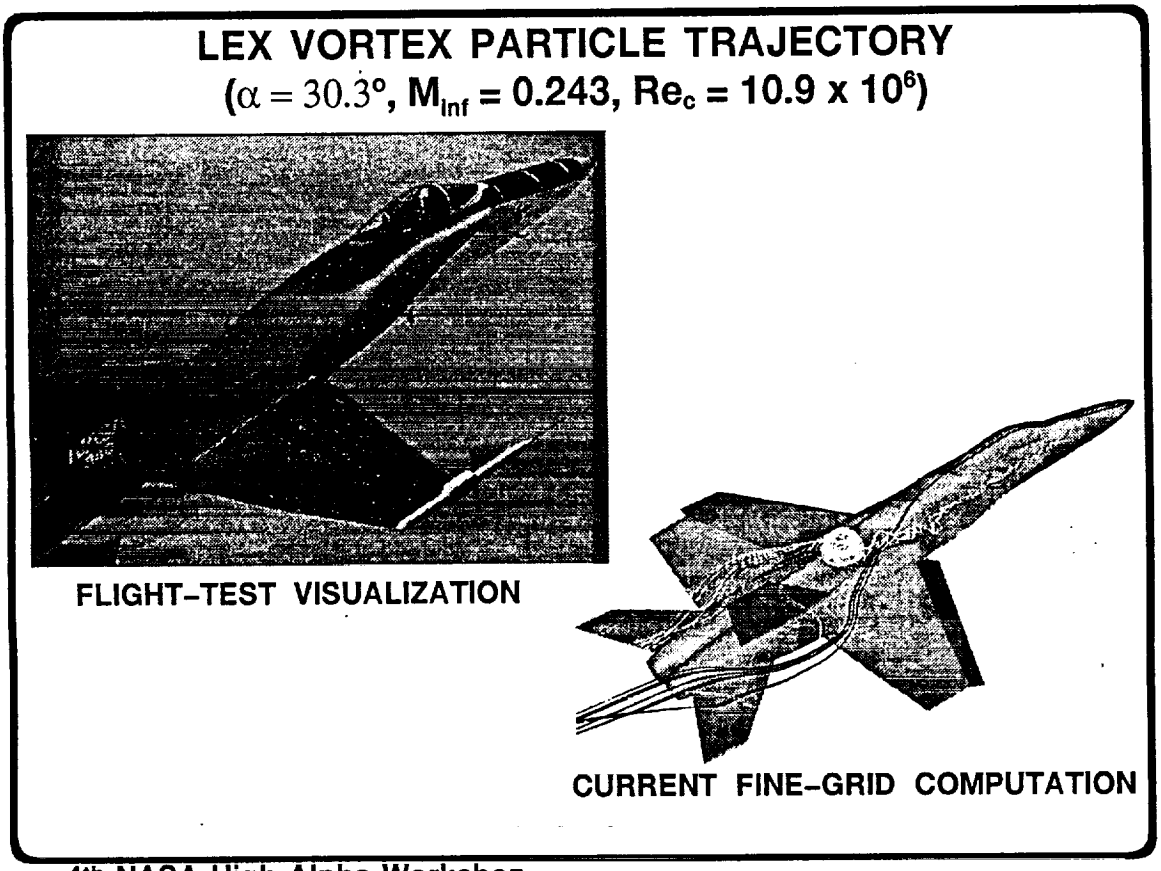

Here, the computed surface pressure distribution on the fuselage forebody at axial stations corresponding to the F–18 HARV pressure port locations are shown. The present computed results and previous results obtained on a coarser computational grid are compared to the flight-test data. Both computations show a good agreement with the flight data at all stations on the forebody, including the region of the primary forebody vortices which are seen at F.S. 142 and F.S. 184 near $\phi = 160°$. The discrepancy at $\phi = 90°$ and F.S. 142 is caused by an antenna fairing on the aircraft which is not modeled in the computation.

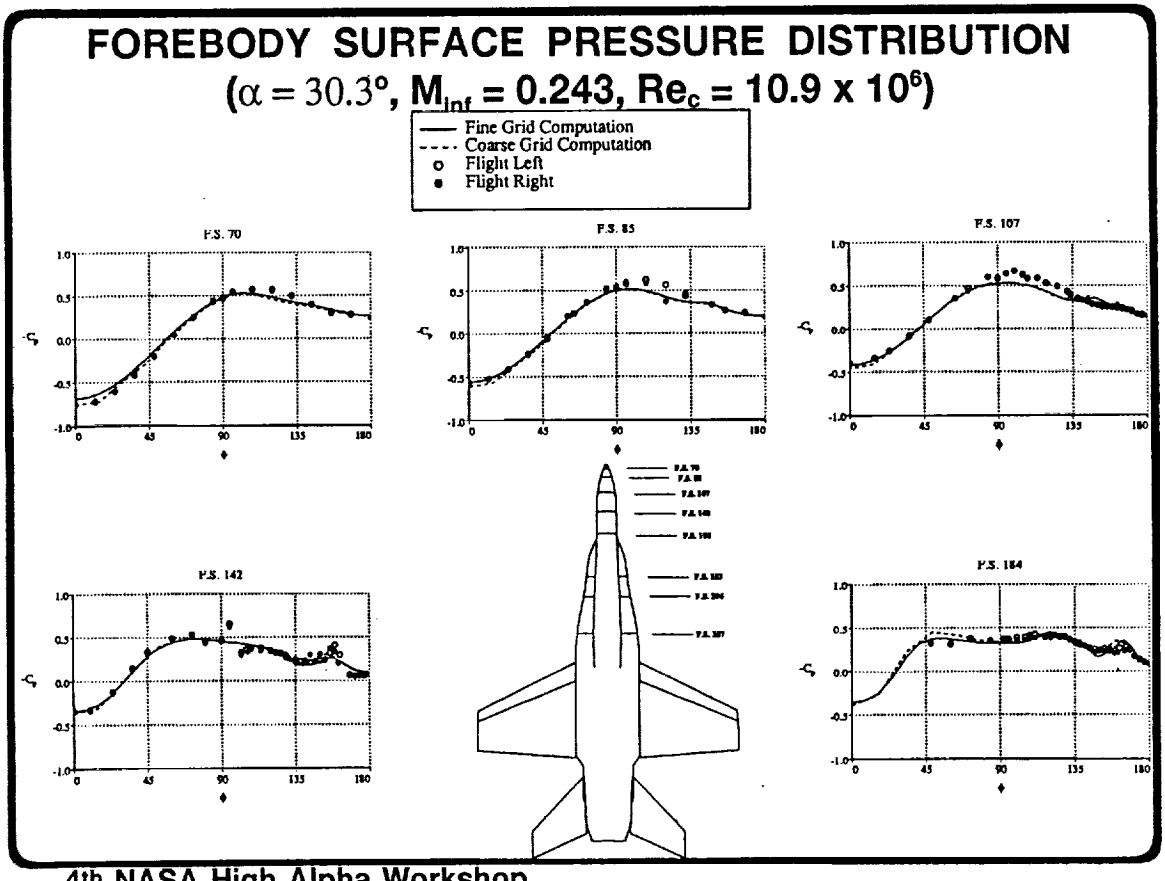

The current computational results show a markedly improved comparison with the flight measurements in the region of the LEX vortex. At F.S. 253 and F.S. 296, upstream of the LEX vortex breakdown position, the present computational suction peaks are in good agreement with the flight measurements. In contrast, the coarser-grid results do not adequately resolve the primary vortex suction peak. At $\alpha = 30°$, vortex breakdown occurs on the aircraft at a fuselage station of F.S. $\approx$ 335. This results in the change in the shape of the pressure distribution between that measured at F.S. 296 and that measured at F.S. 357 in the flight data . The present computations indicate that vortex breakdown occurs at F.S. $\approx$ 375, aft of that observed in the flight testing. Thus, the comparison between computation and flight at F.S. 357 are not in as good agreement. Note that the coarser-grid solutions indicate vortex breakdown occurs at F.S. $\approx$ 435, even farther aft of the actual breakdown position, and the vortex suction peak for the coarser-grid computation remains high between F.S. 296 and F.S. 357.

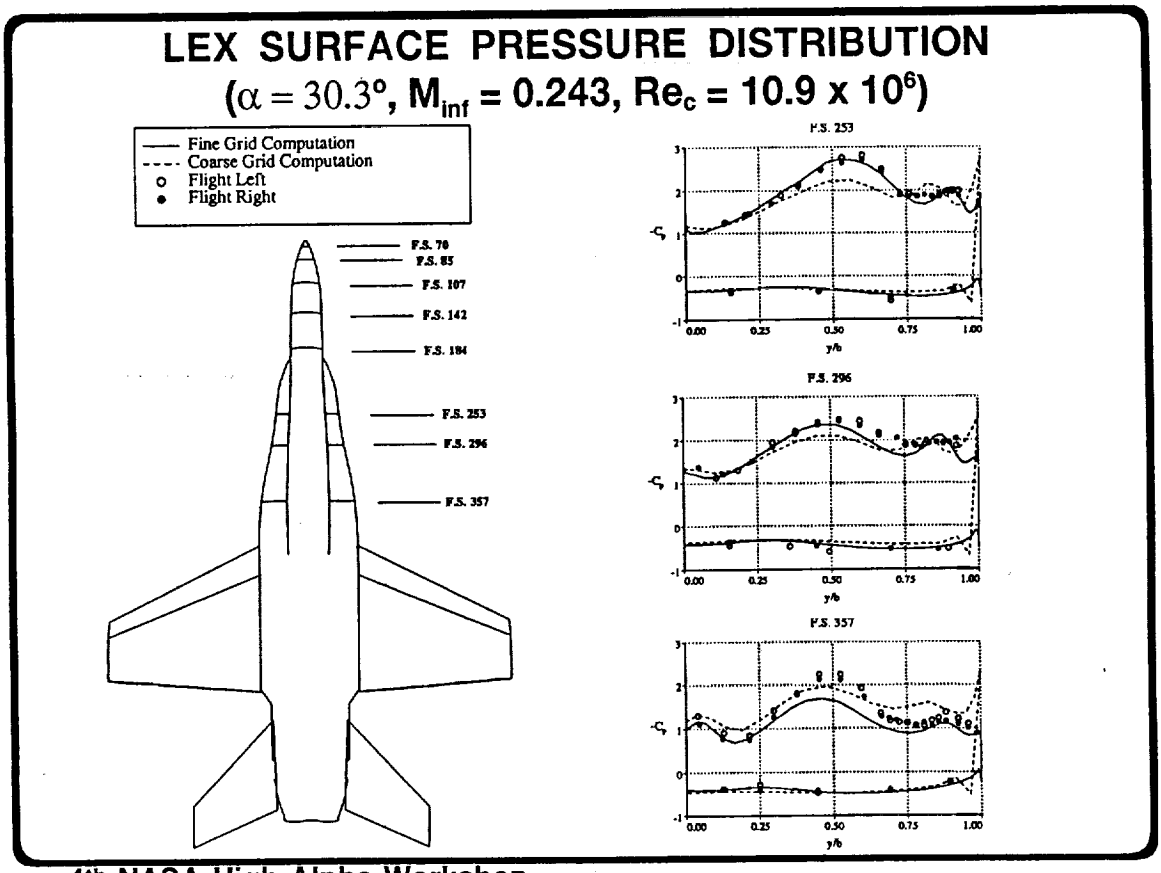

The current computational model has also been used to compute the flow about the F–18 HARV at 45° angle of attack. At $\alpha = 45°$, the HARV forebody flow was found to contain relatively large regions of laminar and transitionary flow, extending approximately 4 ft. aft from the tip of the nose (cf. Fisher et al. "In-Flight Flow Visualization Characteristics of the NASA F–18 High Alpha Research Vehicle at High Angles of Attack," NASA TM 4193). In order to promote transition and thus contract this region, the HARV was also flown with transition strips applied along the forebody. The flowfield at this higher angle of attack has been computed as fully turbulent, and the accuracy of this approximation is evaluated by comparison with flight-test data having both natural transition, and forced transition using the fuselage strips.

FLIGHT–TEST SURFACE FLOW VISUALIZATION α = 47°

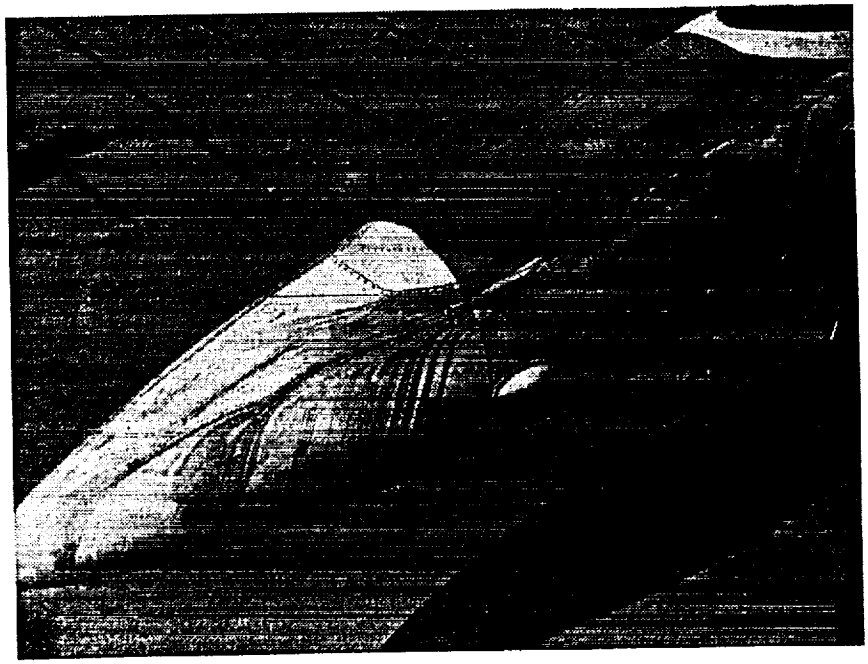

The computed surface pressure distributions on the fuselage forebody at $\alpha = 45°$ are compared to the flight data obtained allowing natural transition on the forebody. The computed results show a good agreement with the flight data at all stations on the windward side of the body where the boundary layer remains attached. On the leeward side of the body ($\phi = 135° - 190°$), the agreement is not as good at the first three axial locations. A strong primary vortex suction peak is seen in the computations, but does not appear in the flight-test data until F.S. 142. This discrepancy is likely due to the assumption of fully turbulent flow which is made in the computations.

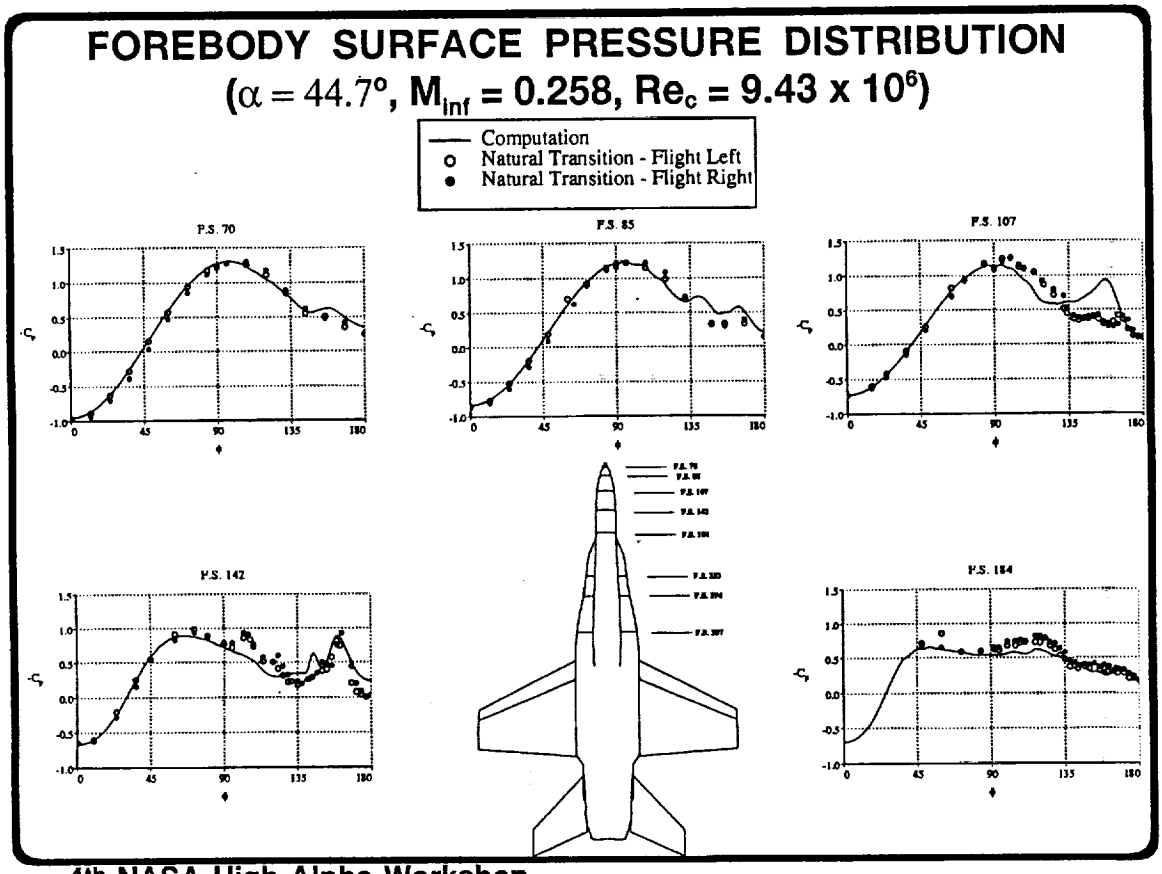

Here, the computed surface pressure distributions at $\alpha = 45°$ are compared to the flight-test data that was obtained with the transition strips in place. The comparison of the computed results with the flight data is improved, especially at F.S. 107, where the flight data with forced transition shows a primary vortex suction peak has formed. At the stations further downstream of the nose the flow is more nearly fully turbulent, and the accuracy of the fully turbulent computations improves. Again, an antenna fairing is present near $\phi = 90°$ at F.S. 142 on the aircraft.

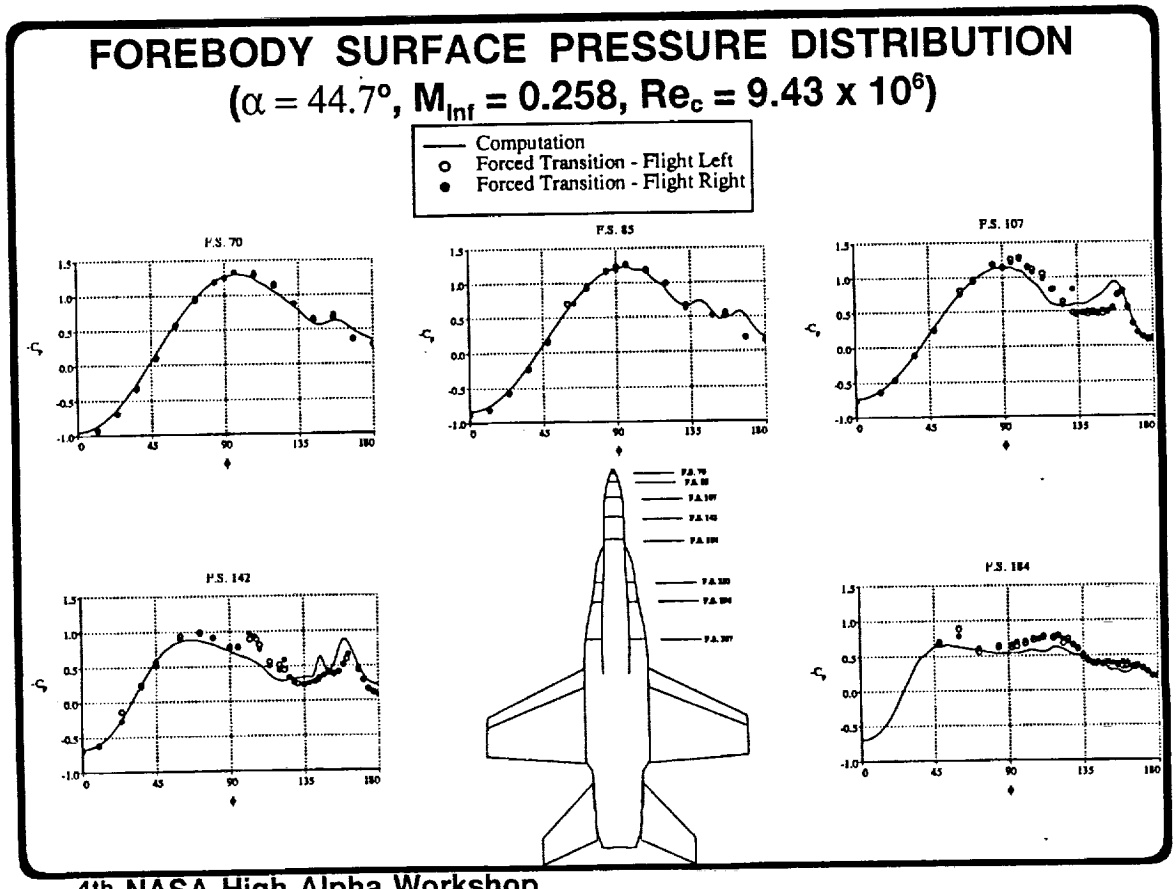

The computed LEX vortex breakdown position is compared to the measured vortex breakdown in the flight tests. The current computational model shows an improvement in the predicted breakdown position. At $\alpha = 45°$, the LEX vortex breaks down very near the apex of the LEX.

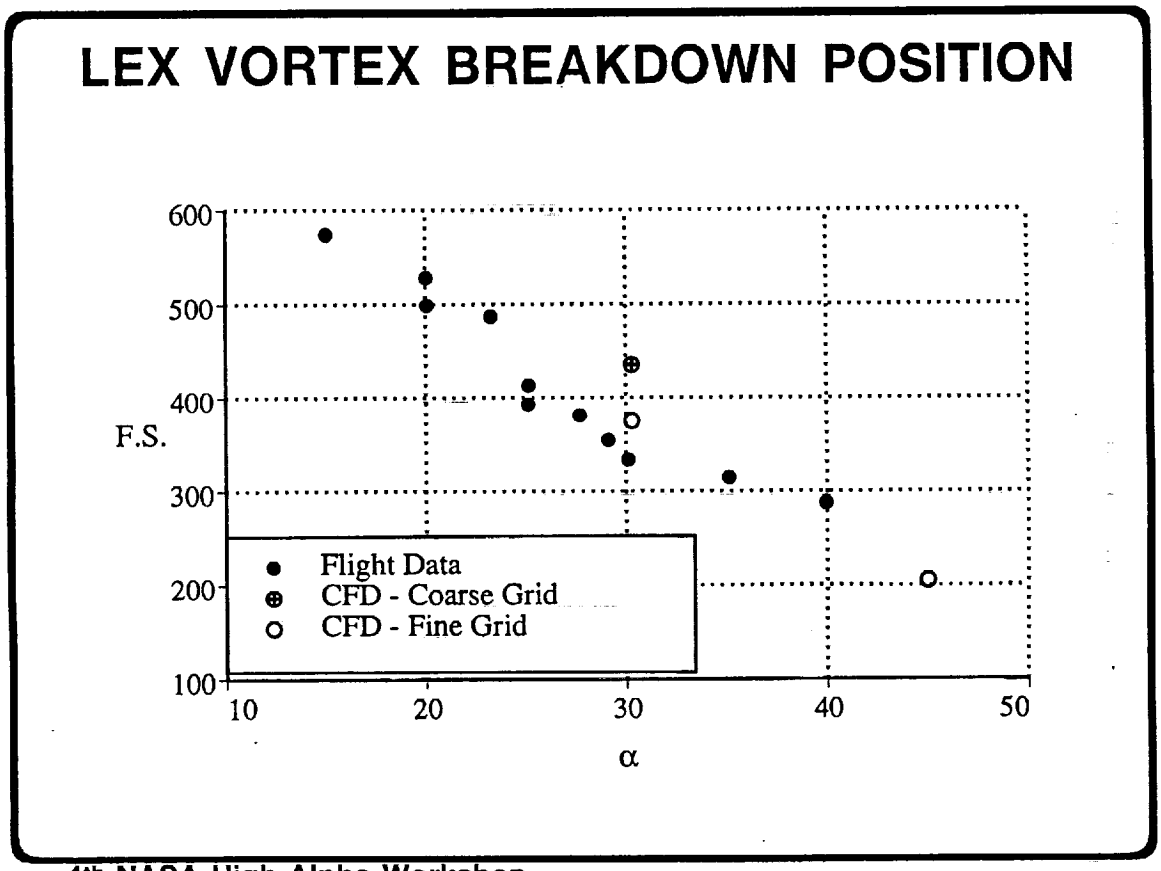

At sufficiently high angles of attack, vortex asymmetries can form over the F–18 and induce dynamic motions such as wing rock. Recently, numerical methods similar to those used in the F–18 computations have been used to investigate aerodynamic-induced roll motions. This view graph presents an overview of the research done by Chaderjian and Schiff for a 65° sweep delta wing[1]. The results of two dynamic computations are presented, one a large-amplitude, high-rate forced-roll motion, and the second a damped free-to-roll motion. The free-to-roll motion is computed by coupling the Navier-Stokes equations with the flight dynamic equation of roll motion. In the forced-roll case, the computed and experimental dynamic rolling-moment coefficients (C_l) are in good agreement with each other. The area enclosed by a dynamic C_l curve indicates the amount of work done by the fluid on the wing. The computation shows a larger enclosed area than the experiment, indicating that the computation is more highly damped. The effect of increased damping can be seen in the free-to-roll case as the computed time-history of rolling angle agrees well with the experimental data in the first half-cycle, then decays more rapidly. The computed and experimental frequencies are in good agreement.

[1] Chaderjian, N.M. and Schiff, L.B.,"Navier-Stokes Prediction of Large-Amplitude Forced and Free-to-Roll Delta-Wing Oscillations," AIAA Paper 94–1884, June, 1994.

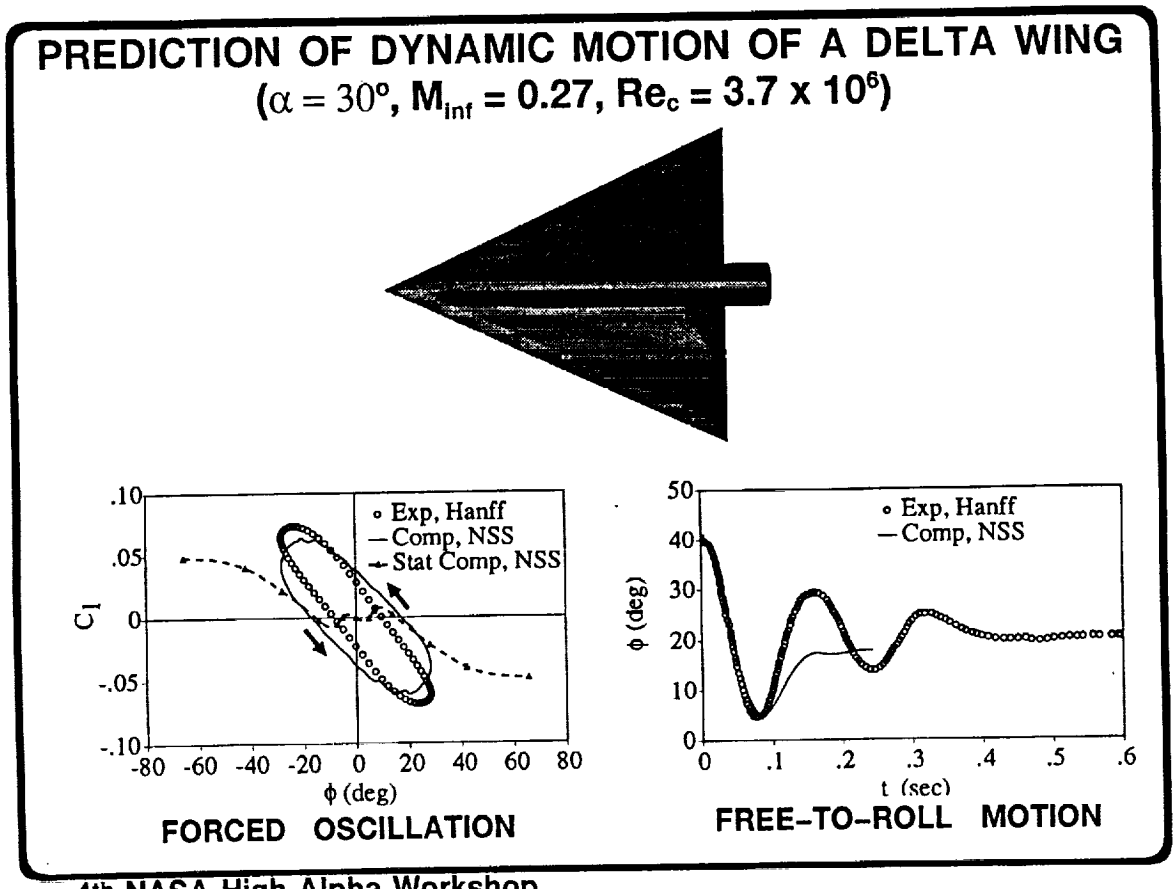

Prior to computing the full-aircraft configuration at higher angles of attack ($\alpha = 60°$ and 70°), computations were carried out for the simpler geometry of an ogive-cylinder. The results of these computations show that at $\alpha = 60°$ the ogive-cylinder develops a numerically-induced lateral force. This lateral force does not appear in the similar $\alpha = 40°$ computation. It is important to understand the cause of this behavior before undertaking a more complex full-aircraft computation at $\alpha = 60°$. Research is currently investigating the source of this numerical asymmetry and means of its alleviation.

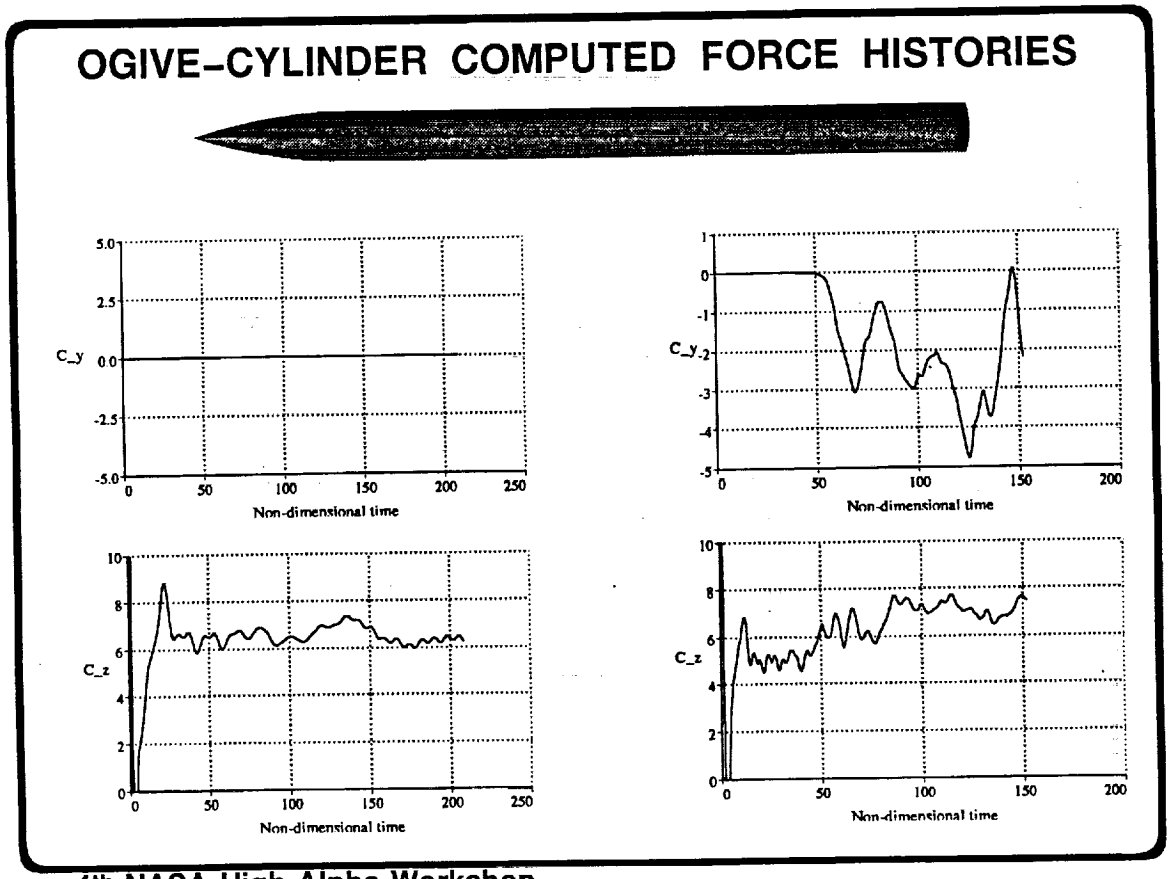

The computational results for the flow about the F–18 HARV at $\alpha = 30°$ show both a good qualitative and quantitative agreement with the flight-test data. The current computational model was able to resolve the details of the forebody and LEX surface flow pattern, better predict the suction peak due to the primary LEX vortex, and improve the predicted position of vortex breakdown. The computations carried out at $\alpha = 45°$ conditions show a good agreement with the flight-data, although the correlation is not as favorable as at $\alpha = 30°$. This is primarily due to the assumption of a fully turbulent flowfield in the computations, while the actual flow contains significant laminar and transitional regions. Finally, similar numerical methods have been used to compute the flow about a delta wing in roll motions.

SUMMARY

* COMPUTATIONS AT α = 30° SHOW IMPROVED CORRELATION WITH FLIGHT–TEST DATA
  * DETAILS OF THE FOREBODY AND LEX SURFACE FLOW PATTERN
  * PREDICTION OF THE LEX PRESSURE DISTRIBUTION
  * PREDICTION OF THE LEX VORTEX BREAKDOWN POSITION
* COMPUTATIONS AT α = 45° SHOW A GOOD AGREEMENT WITH THE FLIGHT–TEST PRESSURE DATA, THOUGH NOT AS FAVORABLE AS THE COMPARISON AT 30°
* SIMILAR NUMERICAL METHODS HAVE BEEN SUCCESSFULLY APPLIED TO THE PREDICTION OF DYNAMIC ROLL MOTIONS AT HIGH–ALPHA FLIGHT CONDITIONS

The areas that are currently being investigated are the development of a transition model suitable for use in high-alpha flows about slender bodies, and the cause of the numerical asymmetry that develops in computations about ogive-cylinder configurations at $\alpha = 60°$. When these issues are resolved, it is intended that the flowfield about the full F–18 aircraft will be re-computed at $\alpha = 45°$ and a computation will be undertaken at $\alpha = 60°$.

FUTURE RESEARCH

* DEVELOP A TRANSITION MODEL FOR HIGH–ALPHA FLOWFIELDS AND APPLY IT TO THE F–18 HARV FUSELAGE FOREBODY

* RESOLVE THE SOURCE AND INFLUENCE OF THE NUMERICALLY INDUCED ASYMMETRIC FLOW DEVELOPED ABOUT OGIVE–CYLINDER CONFIGURATIONS AT α = 60°

* COMPUTE THE FLOW ABOUT THE F–18 HARV AT 45° AND 60° ANGLE OF ATTACK

The current research is aimed at developing and extending numerical methods to accurately predict the high Reynolds number flow about the NASA F–18 HARV at large angles of attack. The resulting codes are validated by comparison of the numerical results with in-flight aerodynamic measurements and flow visualization obtained on the HARV. Further, computations have been used to provide an analysis and numerical optimization of a pneumatic slot blowing concept, and a mechanical strake concept, for use as potential forebody flow control devices in improving high-alpha maneuverability (cf. Gee, et al. These proceedings).

MOTIVATION

* PROVIDE FLIGHT–VALIDATED NUMERICAL METHODS FOR COMPUTING THE FLOW ABOUT AIRCRAFT OPERATING IN THE HIGH–APLHA REGIME

* USE THESE METHODS TO PROVIDE AN ANALYSIS AND OPTIMIZATION OF NEW CONTROL CONCEPTS FOR HIGH–ALPHA MANEUVERABILITY

Computation of the flow about the F–18 HARV at high alpha provides a challenge for numerical methods because of the complex physics involved and the complex geometry of a full-aircraft configuration. Since the computations are carried out to match actual flight operating conditions, the Navier-Stokes equations must be solved. Further, the flow about the majority of the aircraft is turbulent, and the computations must include suitable turbulence models. These models must be applied in a rational manner to account for the massive 3–D separation that occurs at large incidence. The complex aircraft geometry is modeled using structured, overlapped grids in what is termed a Chimera approach. This method allows grids to be generated about the separate components of the aircraft and then combined, greatly simplifying the grid generation procedure. This approach also allows the use of different numerical schemes in different regions of the aircraft, depending upon the physics encountered.

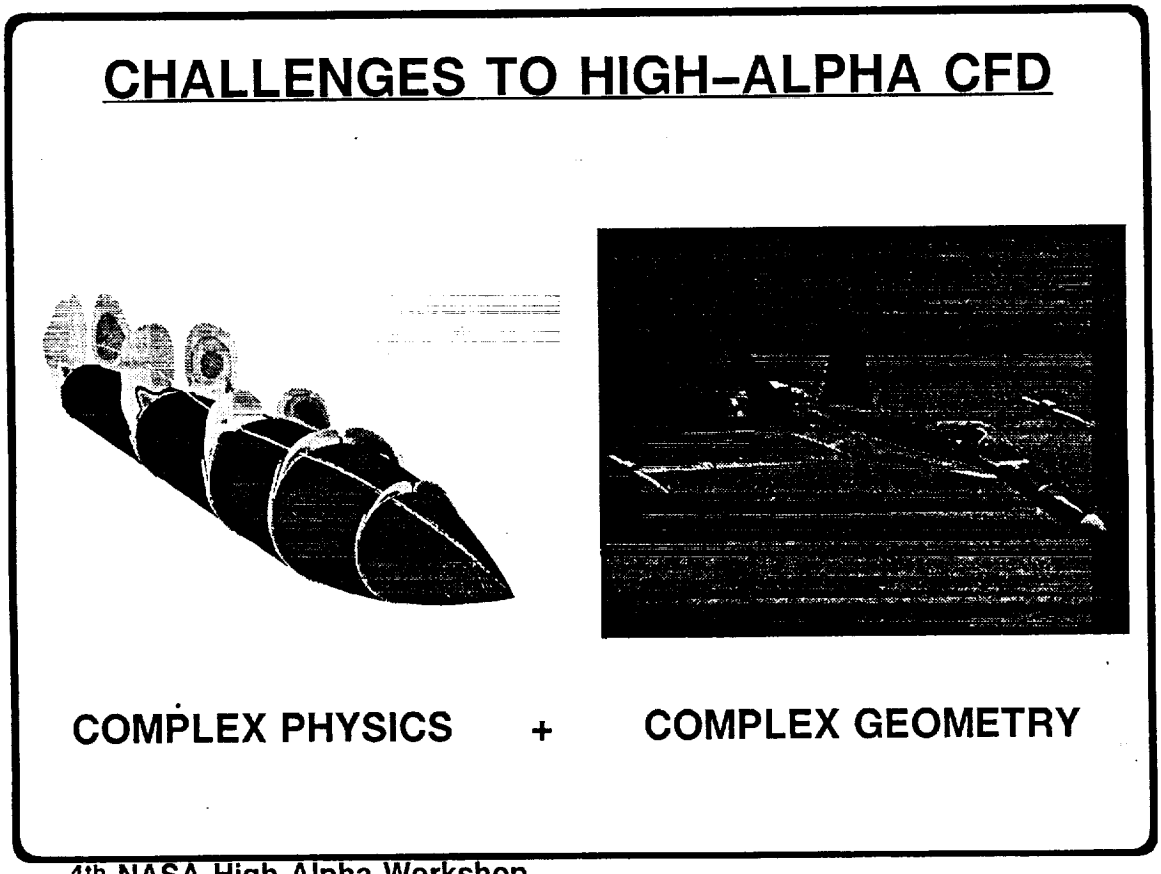

The computational model of the F–18 HARV is a continuing evolution of previous models. The current model has a finer grid spacing in the fuselage and LEX regions, and resolves the engine inlet region is greater detail. The figure shows the separate grids about the major components of the aircraft and how they overlap in the Chimera approach. The model contains 1.7 million grid points in 14 separate zones (15 zones for the $\alpha = 45°$ computations). It models all of the major components of the HARV, including the LEX, wing and leading-edge flap, and the horizontal and vertical tails. The wing-leading-edge flap and horizontal stabilizer are both scheduled with angle of attack in the computations.

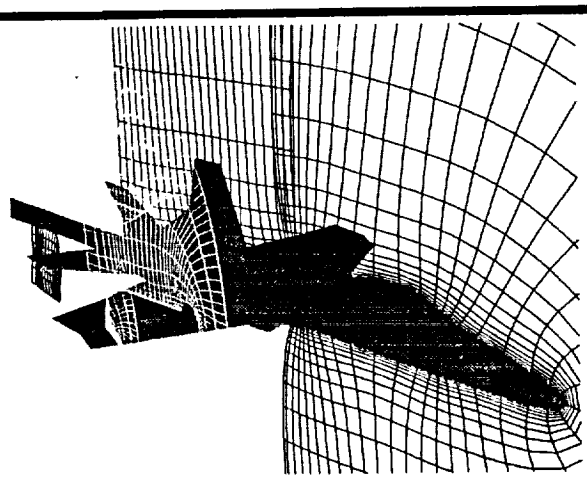

CURRENT F–18 COMPUTATIONAL MODEL

* 1.7 MILLION GRID POINTS FOR A SYMMETRIC COMPUTATION
* 14 STRUCTURED ZONES (13 NAVIER–STOKES)
* MODELS LEX, EMPENNAGE, DEFLECTED FLAP, AND INLET REGION
* MATCHES IN–FLIGHT ENGINE MASS FLOW RATES

This figure shows a close-up view of the engine inlet region of the HARV computational geometry. The major details of the region are modeled, including the boundary layer diverter and vent, and the engine cowling and diffuser. At the engine compressor face, a nozzle is added which forces the flow to choke at the throat of the nozzle. In this manner, different engine inlet mass flow rates can be simulated by opening or constricting the throat of this nozzle. The current computations are carried out at the maximum engine power setting in all cases ($\approx$ 60 lbm/sec per engine).

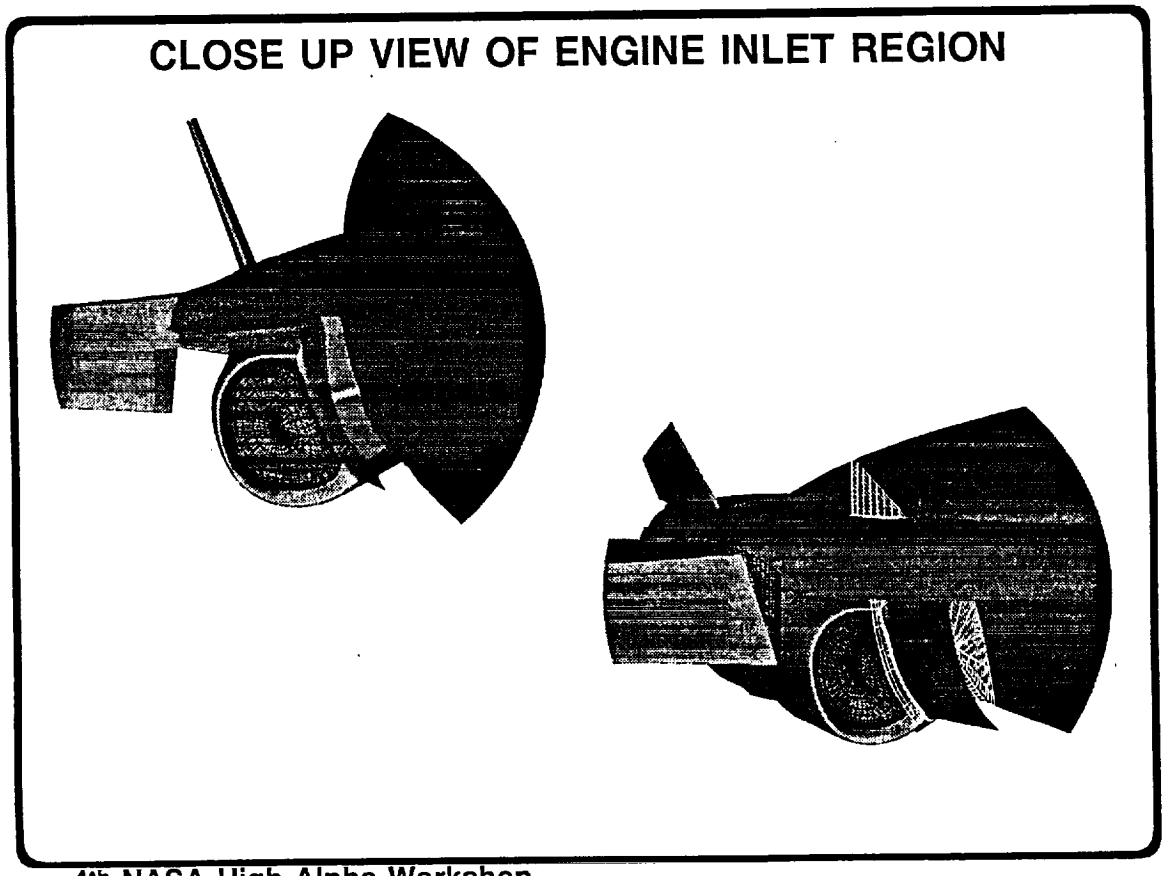

This view graph compares the computed and flight-test oil-flow patterns on the F–18 forebody and LEX at $\alpha = 30°$. The computations were carried out using the full-aircraft configuration. The HARV oil-flow pattern shows the lines of primary and secondary crossflow separation on the fuselage forebody. A primary crossflow separation occurs at the leading edge of the LEX, and the oil flow photo shows lines of secondary and tertiary separation on the upper surface of the LEX. The current computation shows an improvement in the resolution of the forebody secondary separation in comparison to that of a previous solution. The current computation also resolves the details of the secondary and tertiary separation patterns on the leeward side of the LEX. In addition, details of an additional primary and secondary crossflow separation pattern located on the side of the fuselage under the LEX can be seen in the present solution.

FUSELAGE SURFACE FLOW VISUALIZATION

($\alpha = 30.3°$, $M_{inf} = 0.243$, $Re_c = 10.9 \times 10^6$)

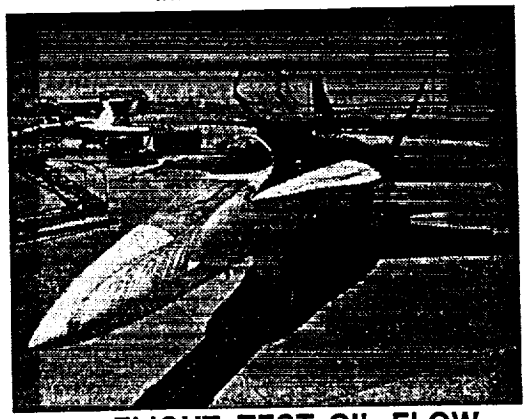

FLIGHT–TEST OIL FLOW

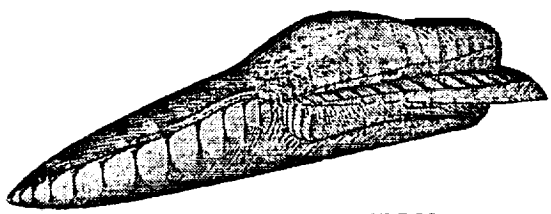

PREVIOUS COMPUTATION

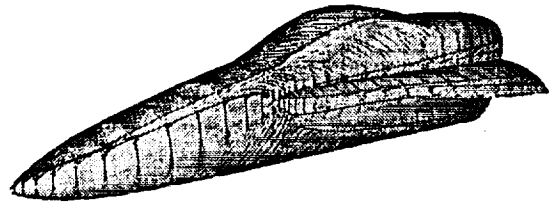

CURRENT COMPUTATION

Particle trajectories (instantaneous streaklines) released from the tip of the forebody and the apex of the LEX in the present $\alpha = 30°$ computation show the path of the forebody and LEX vortices. The flight-test smoke flow visualization is shown for comparison. The slow expansion of the vortex core upstream of breakdown, and the loss of core structure starting in the vicinity of the LEX-wing junction can be seen. The computed vortex breakdown occurs slightly further downstream than is observed in flight.

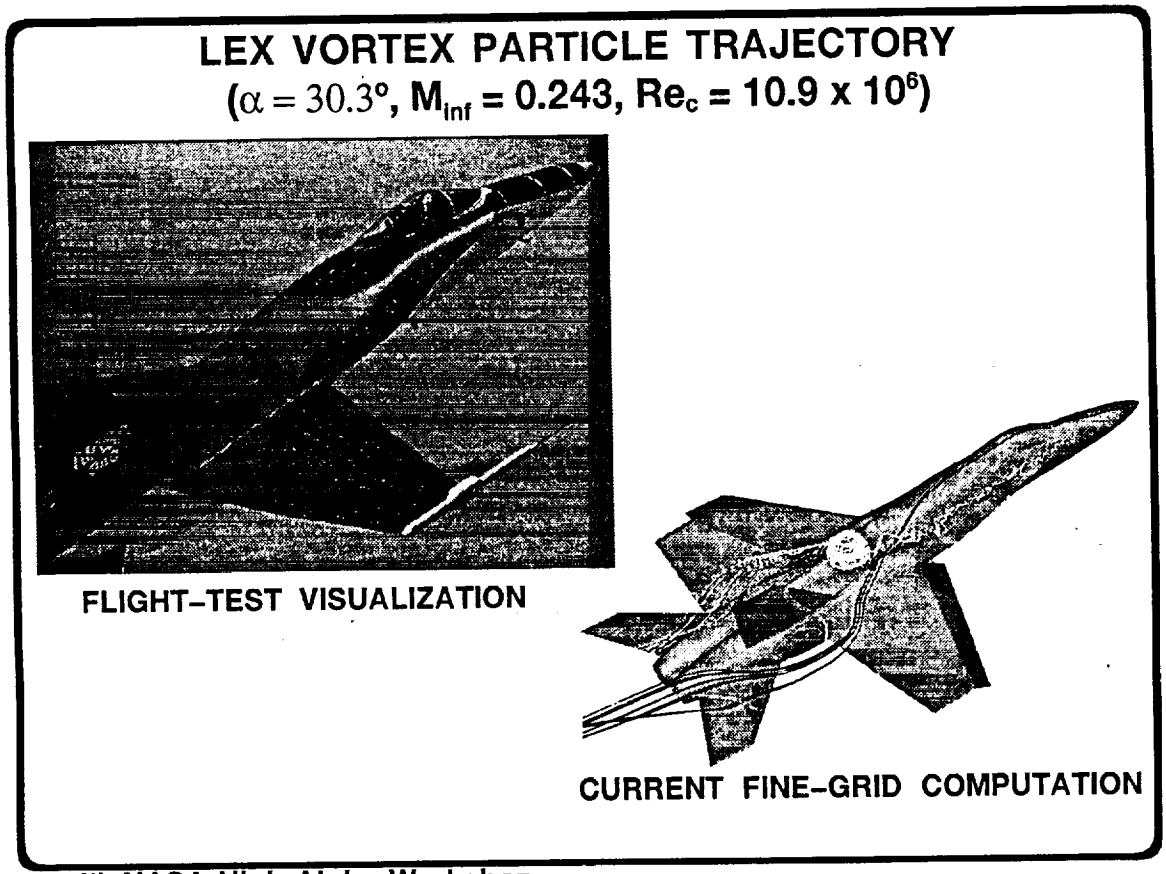

Here, the computed surface pressure distribution on the fuselage forebody at axial stations corresponding to the F–18 HARV pressure port locations are shown. The present computed results and previous results obtained on a coarser computational grid are compared to the flight-test data. Both computations show a good agreement with the flight data at all stations on the forebody, including the region of the primary forebody vortices which are seen at F.S. 142 and F.S. 184 near $\phi = 160°$. The discrepancy at $\phi = 90°$ and F.S. 142 is caused by an antenna fairing on the aircraft which is not modeled in the computation.

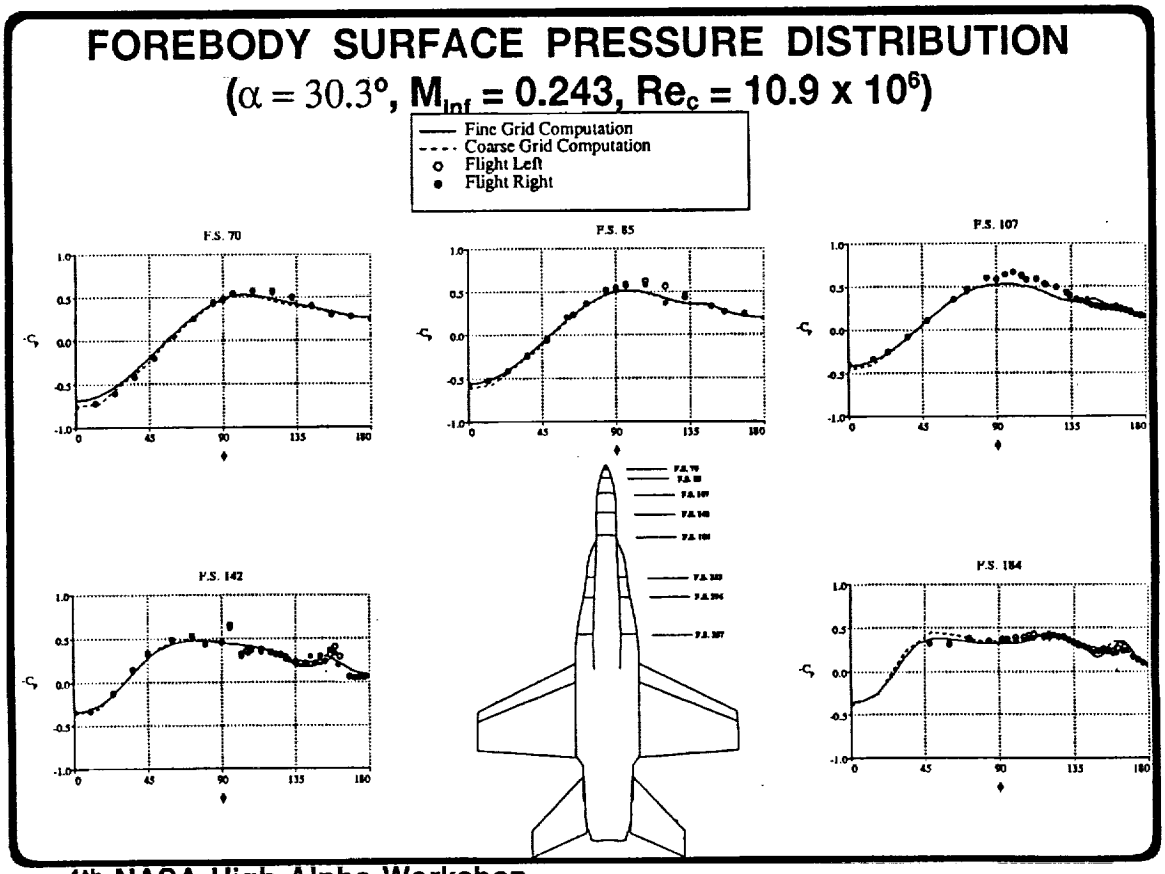

The current computational results show a markedly improved comparison with the flight measurements in the region of the LEX vortex. At F.S. 253 and F.S. 296, upstream of the LEX vortex breakdown position, the present computational suction peaks are in good agreement with the flight measurements. In contrast, the coarser-grid results do not adequately resolve the primary vortex suction peak. At $\alpha = 30°$, vortex breakdown occurs on the aircraft at a fuselage station of F.S. $\approx$ 335. This results in the change in the shape of the pressure distribution between that measured at F.S. 296 and that measured at F.S. 357 in the flight data . The present computations indicate that vortex breakdown occurs at F.S. $\approx$ 375, aft of that observed in the flight testing. Thus, the comparison between computation and flight at F.S. 357 are not in as good agreement. Note that the coarser-grid solutions indicate vortex breakdown occurs at F.S. $\approx$ 435, even farther aft of the actual breakdown position, and the vortex suction peak for the coarser-grid computation remains high between F.S. 296 and F.S. 357.

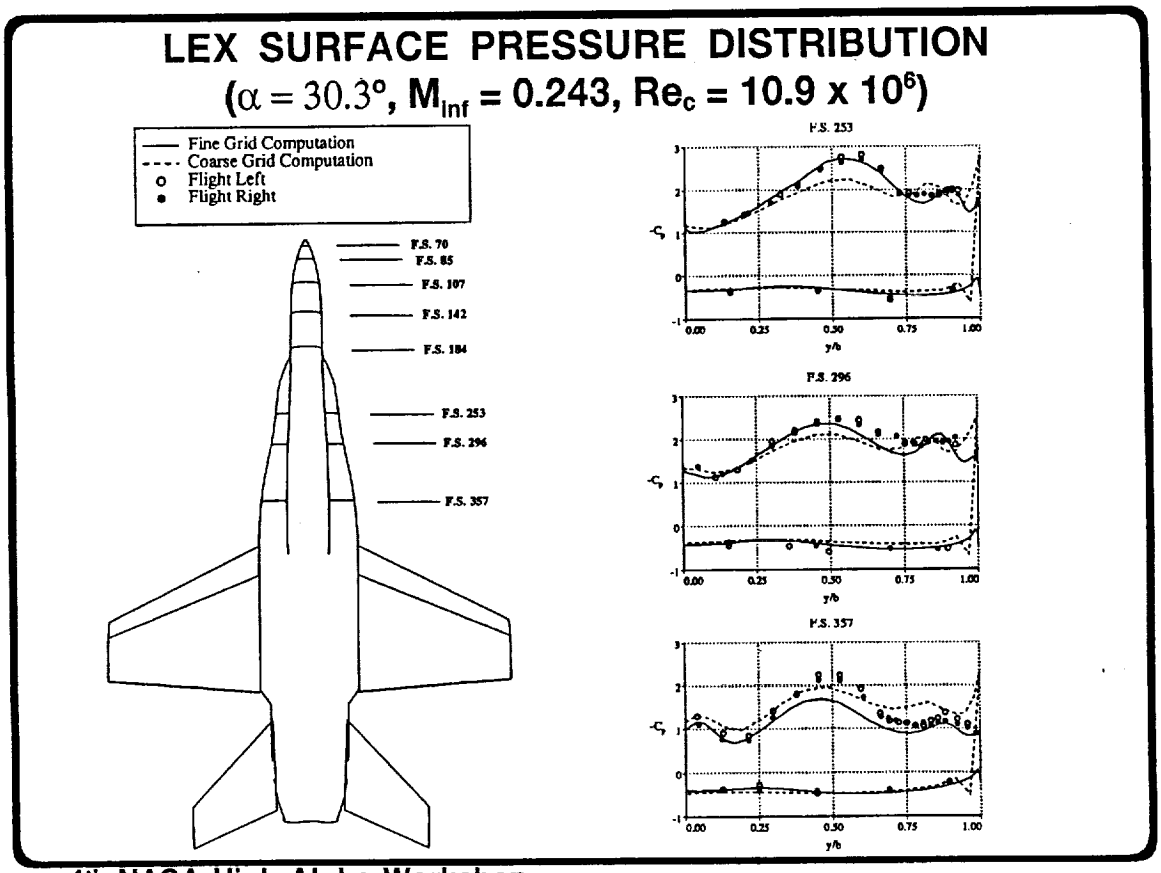

The current computational model has also been used to compute the flow about the F–18 HARV at 45° angle of attack. At $\alpha = 45°$, the HARV forebody flow was found to contain relatively large regions of laminar and transitionary flow, extending approximately 4 ft. aft from the tip of the nose (cf. Fisher et al. "In-Flight Flow Visualization Characteristics of the NASA F–18 High Alpha Research Vehicle at High Angles of Attack," NASA TM 4193). In order to promote transition and thus contract this region, the HARV was also flown with transition strips applied along the forebody. The flowfield at this higher angle of attack has been computed as fully turbulent, and the accuracy of this approximation is evaluated by comparison with flight-test data having both natural transition, and forced transition using the fuselage strips.

FLIGHT–TEST SURFACE FLOW VISUALIZATION α = 47°

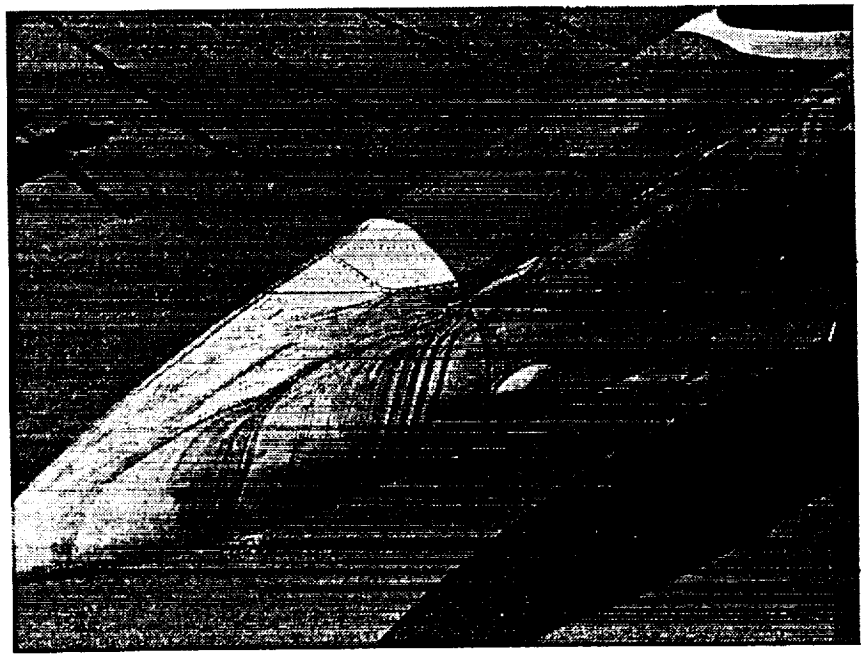

The computed surface pressure distributions on the fuselage forebody at $\alpha = 45°$ are compared to the flight data obtained allowing natural transition on the forebody. The computed results show a good agreement with the flight data at all stations on the windward side of the body where the boundary layer remains attached. On the leeward side of the body ($\phi = 135° - 190°$), the agreement is not as good at the first three axial locations. A strong primary vortex suction peak is seen in the computations, but does not appear in the flight-test data until F.S. 142. This discrepancy is likely due to the assumption of fully turbulent flow which is made in the computations.

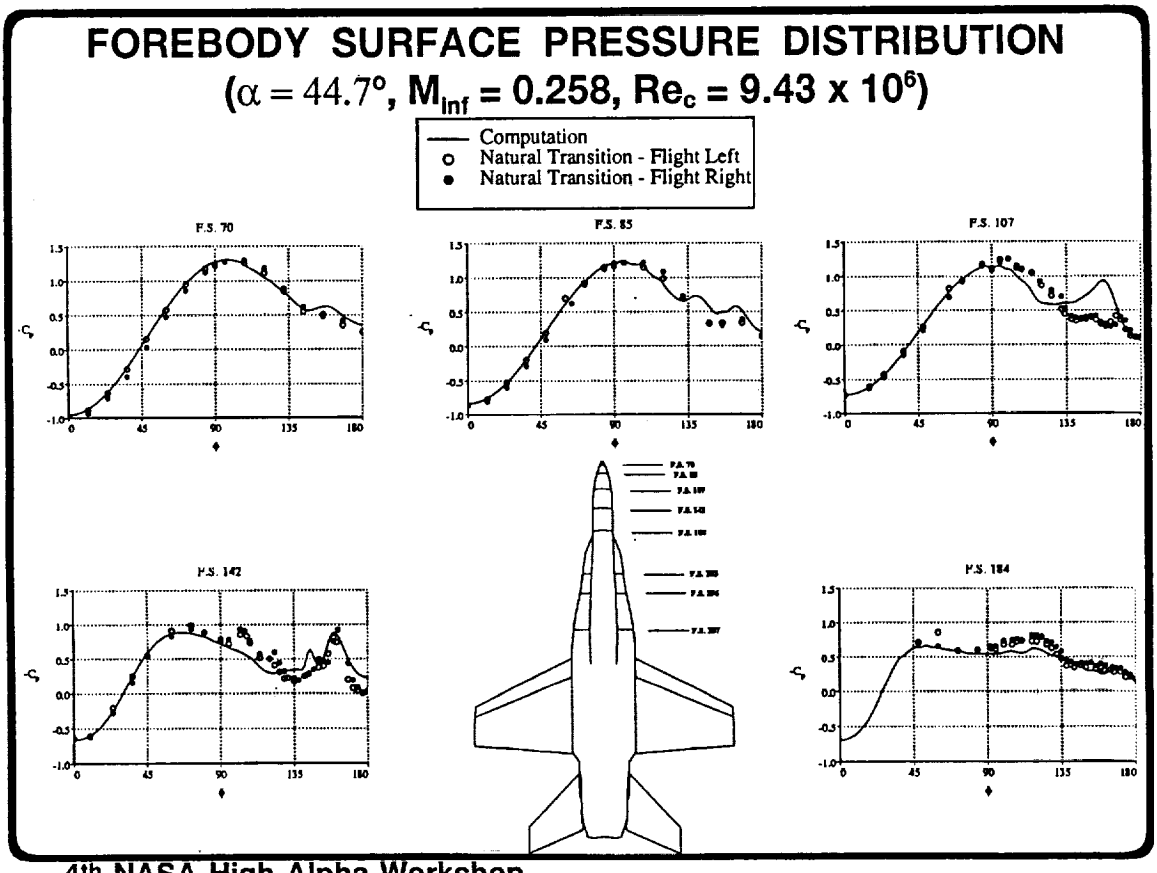

Here, the computed surface pressure distributions at $\alpha = 45°$ are compared to the flight-test data that was obtained with the transition strips in place. The comparison of the computed results with the flight data is improved, especially at F.S. 107, where the flight data with forced transition shows a primary vortex suction peak has formed. At the stations further downstream of the nose the flow is more nearly fully turbulent, and the accuracy of the fully turbulent computations improves. Again, an antenna fairing is present near $\phi = 90°$ at F.S. 142 on the aircraft.

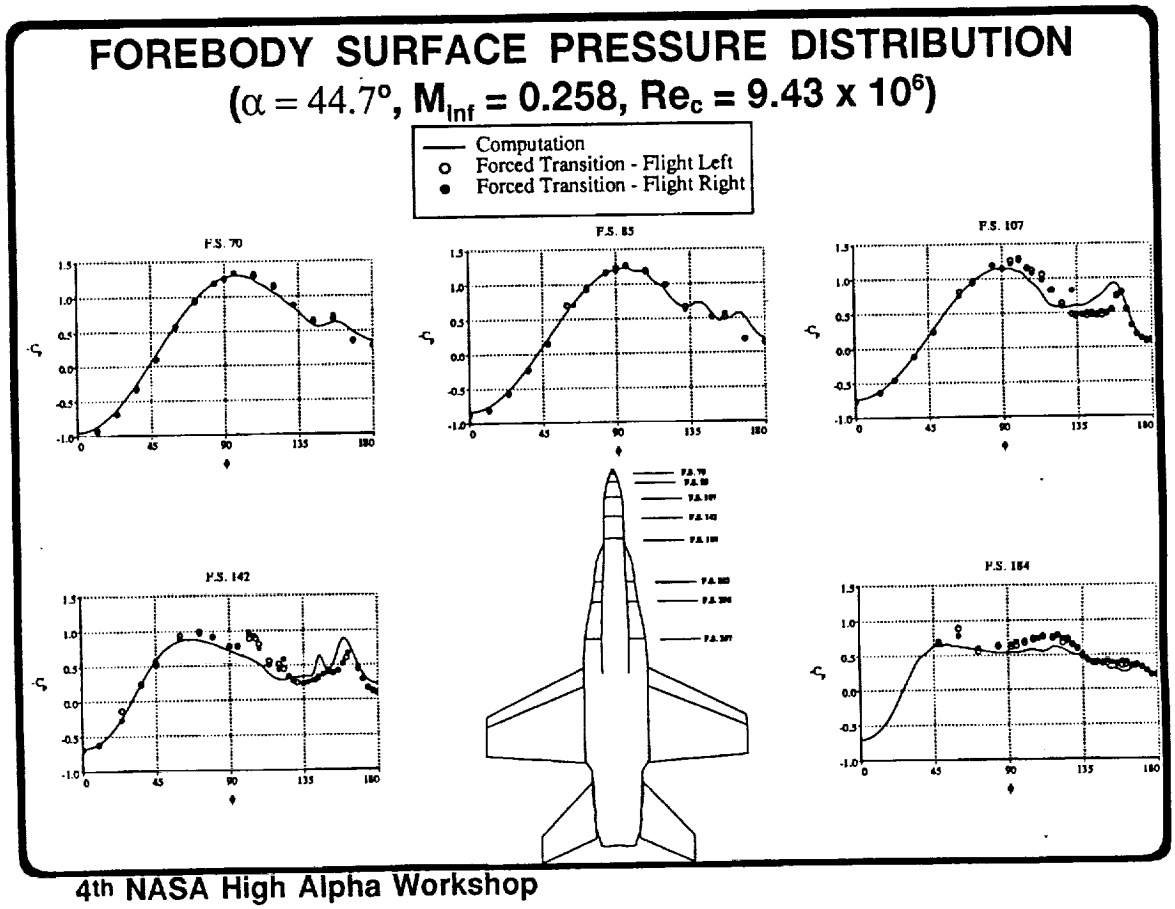

The computed LEX vortex breakdown position is compared to the measured vortex breakdown in the flight tests. The current computational model shows an improvement in the predicted breakdown position. At $\alpha = 45°$, the LEX vortex breaks down very near the apex of the LEX.

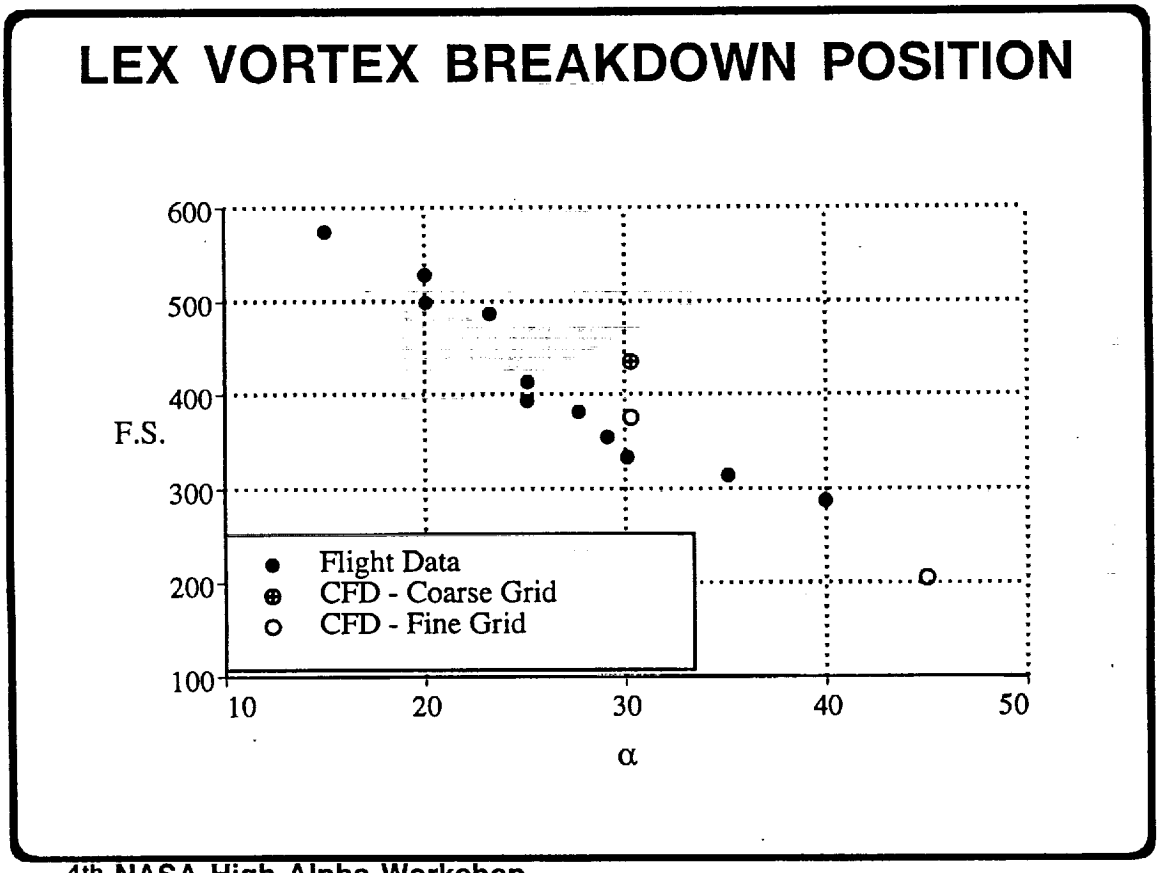

At sufficiently high angles of attack, vortex asymmetries can form over the F–18 and induce dynamic motions such as wing rock. Recently, numerical methods similar to those used in the F–18 computations have been used to investigate aerodynamic-induced roll motions. This view graph presents an overview of the research done by Chaderjian and Schiff for a 65° sweep delta wing[1]. The results of two dynamic computations are presented, one a large-amplitude, high-rate forced-roll motion, and the second a damped free-to-roll motion. The free-to-roll motion is computed by coupling the Navier-Stokes equations with the flight dynamic equation of roll motion. In the forced-roll case, the computed and experimental dynamic rolling-moment coefficients (C_l) are in good agreement with each other. The area enclosed by a dynamic C_l curve indicates the amount of work done by the fluid on the wing. The computation shows a larger enclosed area than the experiment, indicating that the computation is more highly damped. The effect of increased damping can be seen in the free-to-roll case as the computed time-history of rolling angle agrees well with the experimental data in the first half-cycle, then decays more rapidly. The computed and experimental frequencies are in good agreement.

[1] Chaderjian, N.M. and Schiff, L.B.,"Navier-Stokes Prediction of Large-Amplitude Forced and Free-to-Roll Delta-Wing Oscillations," AIAA Paper 94–1884, June, 1994.

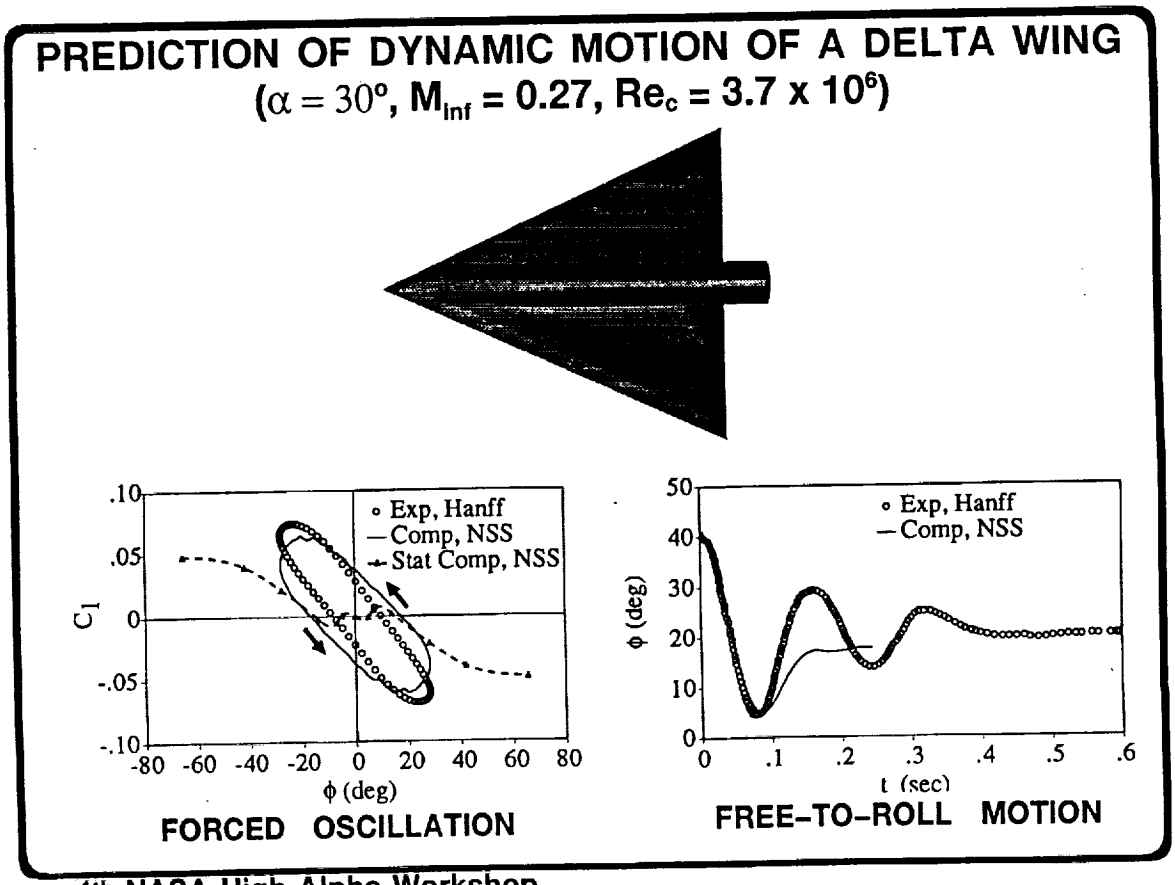

Prior to computing the full-aircraft configuration at higher angles of attack ($\alpha = 60°$ and 70°), computations were carried out for the simpler geometry of an ogive-cylinder. The results of these computations show that at $\alpha = 60°$ the ogive-cylinder develops a numerically-induced lateral force. This lateral force does not appear in the similar $\alpha = 40°$ computation. It is important to understand the cause of this behavior before undertaking a more complex full-aircraft computation at $\alpha = 60°$. Research is currently investigating the source of this numerical asymmetry and means of its alleviation.

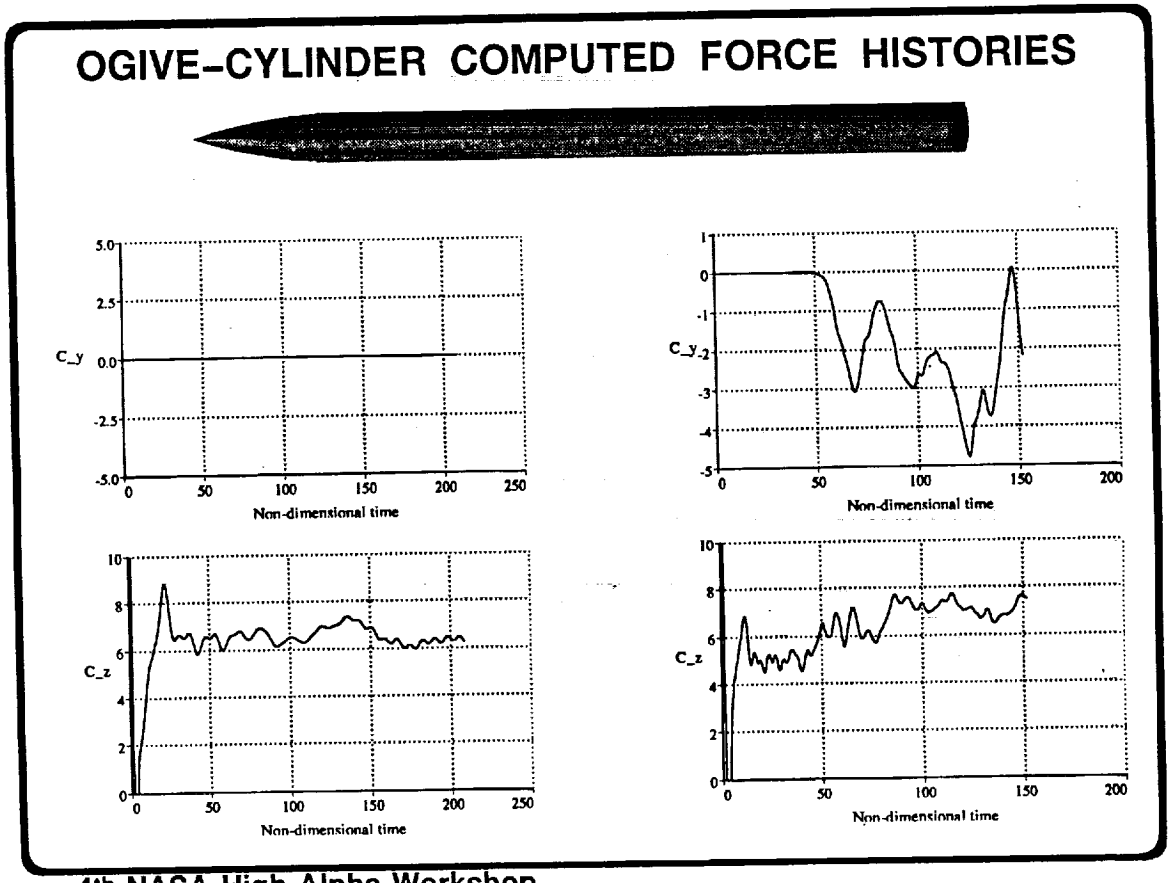

The computational results for the flow about the F-18 HARV at $\alpha = 30°$ show both a good qualitative and quantitative agreement with the flight-test data. The current computational model was able to resolve the details of the forebody and LEX surface flow pattern, better predict the suction peak due to the primary LEX vortex, and improve the predicted position of vortex breakdown. The computations carried out at $\alpha = 45°$ conditions show a good agreement with the flight-data, although the correlation is not as favorable as at $\alpha = 30°$. This is primarily due to the assumption of a fully turbulent flowfield in the computations, while the actual flow contains significant laminar and transitional regions. Finally, similar numerical methods have been used to compute the flow about a delta wing in roll motions.

SUMMARY

* COMPUTATIONS AT α = 30° SHOW IMPROVED CORRELATION WITH FLIGHT-TEST DATA
  * DETAILS OF THE FOREBODY AND LEX SURFACE FLOW PATTERN
  * PREDICTION OF THE LEX PRESSURE DISTRIBUTION
  * PREDICTION OF THE LEX VORTEX BREAKDOWN POSITION
* COMPUTATIONS AT α = 45° SHOW A GOOD AGREEMENT WITH THE FLIGHT-TEST PRESSURE DATA, THOUGH NOT AS FAVORABLE AS THE COMPARISON AT 30°
* SIMILAR NUMERICAL METHODS HAVE BEEN SUCCESSFULLY APPLIED TO THE PREDICTION OF DYNAMIC ROLL MOTIONS AT HIGH-ALPHA FLIGHT CONDITIONS

The areas that are currently being investigated are the development of a transition model suitable for use in high-alpha flows about slender bodies, and the cause of the numerical asymmetry that develops in computations about ogive-cylinder configurations at $\alpha = 60°$. When these issues are resolved, it is intended that the flowfield about the full F–18 aircraft will be re-computed at $\alpha = 45°$ and a computation will be undertaken at $\alpha = 60°$.

FUTURE RESEARCH

* DEVELOP A TRANSITION MODEL FOR HIGH-ALPHA FLOWFIELDS AND APPLY IT TO THE F-18 HARV FUSELAGE FOREBODY

* RESOLVE THE SOURCE AND INFLUENCE OF THE NUMERICALLY INDUCED ASYMMETRIC FLOW DEVELOPED ABOUT OGIVE-CYLINDER CONFIGURATIONS AT α = 60°

* COMPUTE THE FLOW ABOUT THE F-18 HARV AT 45° AND 60° ANGLE OF ATTACK